

Nonchaos-Mediated Mixed-Mode Oscillations in an Enzyme Reaction System

Marcus J. B. Hauser^{*,†} and Jason A. C. Gallas^{‡,||,¶,§}

[†]Abteilung Biophysik, Institut für Experimentelle Physik, Otto von-Guericke-Universität Magdeburg, Universitätsplatz 2, 39106 Magdeburg, Germany

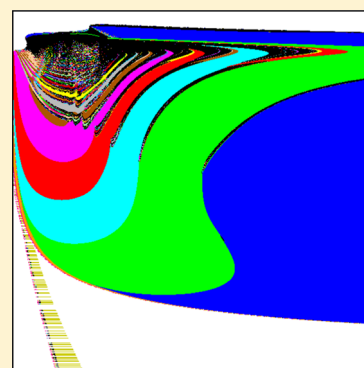
[‡]Departamento de Física, Universidade Federal da Paraíba, 58039-970 João Pessoa, Brazil

^{||}Instituto de Altos Estudos da Paraíba, Rua Infante Dom Henrique 100-1801, 58051-150 João Pessoa, Brazil

[¶]Institute for Multiscale Simulation, Friedrich-Alexander Universität Erlangen-Nürnberg, 91052 Erlangen, Germany

[§]Max Planck Institute for the Physics of Complex Systems, Nöthnitzer Straße 38, 01187 Dresden, Germany

ABSTRACT: We report numerical evidence of a new type of wide-ranging organization of mixed-mode oscillations (MMOs) in a model of the peroxidase–oxidase reaction, in the control parameter plane defined by the supply of the reactant NADH and the pH of the medium. In classic MMOs, the intervals of distinct periodic oscillations are always separated from each other by windows of chaos. In contrast, in the new unfolding, such windows of chaos do not exist. Chaos-mediated and nonchaos-mediated MMO phases are separated by a continuous transition boundary in the control parameter plane. In addition, for low pH values, we find an exceptionally wide and intricate mosaic of MMO phases that is described by a detailed phase diagram.



SECTION: Kinetics and Dynamics

Chemical and biochemical reaction systems are famous for displaying rich varieties of behaviors, including stationary, periodic, self-pulsating, bursting, and chaotic oscillations.^{1–4} Frequently, chemical oscillations appear as mixed-mode oscillations (MMOs), a complex dynamical behavior observed abundantly both numerically and experimentally in numerous prototypical systems. In biological systems, MMOs have potential relevance for signal encoding.^{5–9} MMOs have also been observed in a wide variety of oscillating chemical systems, including homogeneous oscillators,^{10–13} pH oscillators,^{14–16} electrochemical systems,^{1,17–19} and, last but not least, the peroxidase–oxidase (PO) reaction.^{20–24} For recent reviews about MMOs and their applications, see, for example, refs 25 and 26.

MMOs consist of periodic cycles having a number of large peaks intercalated by a number of small peaks in one period of the oscillation. MMOs are commonly represented by a symbol L^S , where L and S denote the numbers of large- and small-amplitude oscillations per cycle, respectively. This standard classification emphasizes the peak multiplicity of the underlying oscillatory time series. An alternative way to classify MMOs is based on the bifurcations leading to mixed-mode behavior by analyzing the slow and fast manifolds along which the oscillations evolve.^{27,28}

MMOs are typically encountered in parameter domains where the dynamics changes from periodic to chaotic oscillations. In particular, the standard MMO route to chaos

involves series with a growing number of peaks having adjacent MMO states L^S and L^{S+1} separated from each other by narrow windows of chaotic dynamics. Because the MMO unfolding scenario comprises multiple transitions between periodic (MMO) and chaotic states, it is obvious that systems displaying MMOs possess rich and intricate control phase diagrams. To date, most studies of MMOs were performed by investigating bifurcation diagrams along specific one-dimensional paths in parameter space, thus providing local information that is often interpolated to yield a global notion of the dynamics. On the other hand, obtaining parameter continuation of bifurcations between MMOs may turn out to be computationally complicated. Furthermore, it is usually rather challenging to try to understand global behaviors by analyzing bifurcation diagrams obtained along just a few isolated one-dimensional paths, particularly for systems governed by many equations and parameters. When mathematical models are known, it is fortunately possible to profit from recent advances in computation to perform detailed calculations of all sorts of oscillatory behaviors of a given reaction system at every point of a control parameter plane of interest.

In this Letter, we report some remarkable phenomena discovered while computing high-resolution phase diagrams for

Received: October 17, 2014

Accepted: November 17, 2014

Published: November 17, 2014

the PO reaction, which is the aerobic oxidation of NADH catalyzed by the enzyme peroxidase. The PO system has a well-studied reaction mechanism²⁹ for which different detailed mathematical models are available.^{30–33} Among them, the mechanism proposed by Bronnikova, Fed'kina, Schaffer, and Olsen³¹ (the so-called BFSO model, Table 1) reproduces with

Table 1. Detailed (BFSO) Model of the PO Reaction^{31a}

	reaction	R_i	rate constants k_i^g
(1)	$\text{NADH} + \text{O}_2 + \text{H}^+ \rightarrow \text{NAD}^+ + \text{H}_2\text{O}_2$	$k_1[\text{NADH}][\text{O}_2]$	3.0^b
(2)	$\text{H}_2\text{O}_2 + \text{Per}^{3+} \rightarrow \text{Per}^{5+} + \text{H}_2\text{O}$	$k_2[\text{H}_2\text{O}_2][\text{Per}^{3+}]$	1.8×10^{7b}
(3)	$\text{Per}^{5+} + \text{NADH} \rightarrow \text{Per}^{4+} + \text{NAD}^*$	$k_3[\text{Per}^{5+}][\text{NADH}]$	4.0×10^{4b}
(4)	$\text{Per}^{4+} + \text{NADH} \rightarrow \text{Per}^{3+} + \text{NAD}^*$	$k_4[\text{Per}^{4+}][\text{NADH}]$	2.6×10^{4b}
(5)	$\text{NAD}^* + \text{O}_2 \rightarrow \text{NAD}^+ + \text{O}_2^-$	$k_5[\text{NAD}^*][\text{O}_2]$	2.0×10^{7b}
(6)	$\text{O}_2^- + \text{Per}^{3+} \rightarrow \text{Per}^{6+}$	$k_6[\text{O}_2^-][\text{Per}^{3+}]$	1.7×10^{7b}
(7)	$2\text{O}_2^- + 2\text{H}^+ \rightarrow \text{H}_2\text{O}_2 + \text{O}_2$	$k_7[\text{O}_2^-]^2$	2.0×10^{7b}
(8)	$\text{Per}^{6+} + \text{NAD}^* \rightarrow \text{Per}^{5+} + \text{NAD}^+$	$k_8[\text{Per}^{6+}][\text{NAD}^*]$	9.0×10^{7b}
(9)	$2\text{NAD}^* \rightarrow \text{NAD}_2$	$k_9[\text{NAD}^*]^2$	variable ^{b,c}
(10)	$\text{Per}^{3+} + \text{NAD}^* \rightarrow \text{Per}^{2+} + \text{NAD}^+$	$k_{10}[\text{Per}^{3+}][\text{NAD}^*]$	1.8×10^{6b}
(11)	$\text{Per}^{2+} + \text{O}_2 \rightarrow \text{Per}^{6+}$	$k_{11}[\text{Per}^{2+}][\text{O}_2]$	1.0×10^{5b}
(12)	$\rightarrow \text{NADH}$	k_{12}	variable ^d
(13)	$\text{O}_2(\text{gas}) \rightarrow \text{O}_2(\text{liquid})$	$k_{13}[\text{O}_2]_{\text{eq}}$	$6.0 \times 10^{-3e,f}$
(-13)	$\text{O}_2(\text{liquid}) \rightarrow \text{O}_2(\text{gas})$	$k_{-13}[\text{O}_2]$	6.0×10^{-3e}

^aRate constants are taken from ref 24. Per^{n+} are the oxidation states of peroxidase: Per^{2+} is ferrous peroxidase; Per^{3+} is ferric peroxidase; Per^{4+} is compound II; Per^{5+} is compound I; and Per^{6+} is compound III. ^bUnits: $\text{M}^{-1} \text{s}^{-1}$. ^cBetween 0 and 1.0×10^8 . ^dBetween 1.0×10^{-7} and $1.40 \times 10^{-7} \text{M s}^{-1}$. ^eUnits: s^{-1} . ^fThe value of $[\text{O}_2]_{\text{eq}}$ is $1.2 \times 10^{-5} \text{M}$. ^gThe concentrations of H^+ are absorbed into the rate constants k_i .

good agreement most of the experimentally observed complex dynamics such as, for example, chaotic oscillations, quasiperiodic oscillations, and MMOs. The BFSO model contains 10

variables (9 of them independent³⁴) and 14 rate constants. Here, we focus on the dynamics observed in experiments,^{23,24} namely, in the control parameter space spanned by the NADH influx rate and the pH value of the medium. The latter is accounted for by lumping the effect of pH changes into a single rate constant, namely, the rate constant k_9 (Table 1) of the pH-dependent dimerization of NAD^* radicals.^{24,35,36} This approach was adopted previously in several studies, where selected bifurcation diagrams in the k_9, k_{12} parameter space were calculated to explain experimental observations.^{24,35,36}

The main findings reported here address three issues concerning the global structural organization of MMOs. First, we report the existence of a new type of MMOs where adjacent L^S are *not* mediated by windows of chaos. This remarkable type of MMOs covers extended domains in control parameter space. Second, we investigate how this nonchaos-mediated MMO phase is connected to the region of classical MMOs, namely, the region where adjacent MMO states are always mediated by windows of chaos. Third, we demonstrate the existence of a large and intricate mosaic of stability phases characterized by chaos-mediated complex oscillations and displaying a peculiar fault running through it (see the white box in Figure 1 and described below).

Figure 1 shows a detailed phase diagram computed according to the BFSO model of the PO reaction, as described in the Computational Details. As can be seen from Figure 1, the BFSO model predicts a rich and systematic organization of the control parameter space spanned by the pH-dependent rate constant of the dimerization of NAD^* radicals (k_9) and the rate of NADH influx (k_{12}).

The classical organization of MMO states can be clearly observed in the upper right part of Figure 1, where series of chaotic windows (black stripes) exist between the domains of periodic oscillations with n spikes (local maxima) per period. For example, classical MMOs were described previously in detail along (i) one-parameter paths like line A, where $k_9 = 4.0 \times 10^7 \text{M}^{-1} \text{s}^{-1}$ is constant and k_{12} varies,²⁴ or (ii) two-parameter paths like B, where both parameters are modified simultaneously according to $k_{12} = -8.8095 \times 10^{-16} \text{M}^2 \times k_9 + 1.4226 \text{M s}^{-1}$.

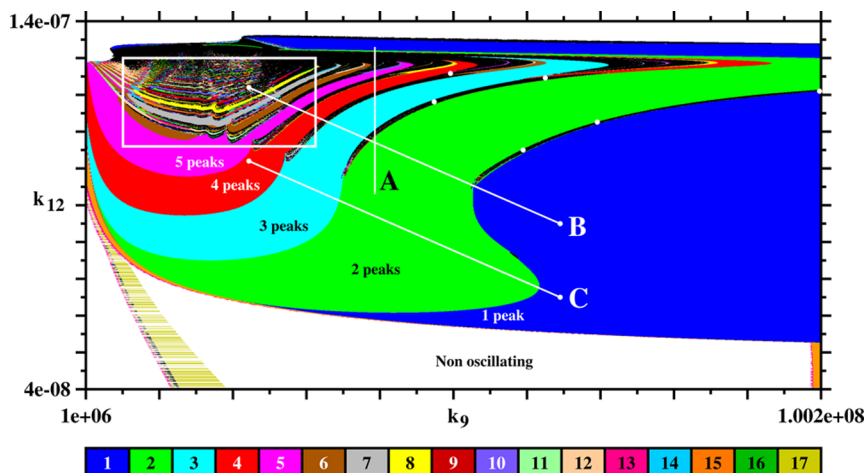


Figure 1. Phase diagram spanned by the rate constant k_9 of the pH-sensitive NAD^* dimerization and the NADH influx rate, k_{12} . The phase diagram displays the number of peaks contained in one period of the periodic oscillations, encoded according to the color bar. White and black denote regions of stationary (nonoscillating) and chaotic oscillations, respectively. As seen from the particular organization of the black stripes of chaos, standard chaos-mediated MMO sequences occur along one-parameter paths like the line A and two-parameter paths like line B. The new nonchaos-mediated MMOs occur along paths like line C. The complex region inside of the box is magnified in Figure 3.

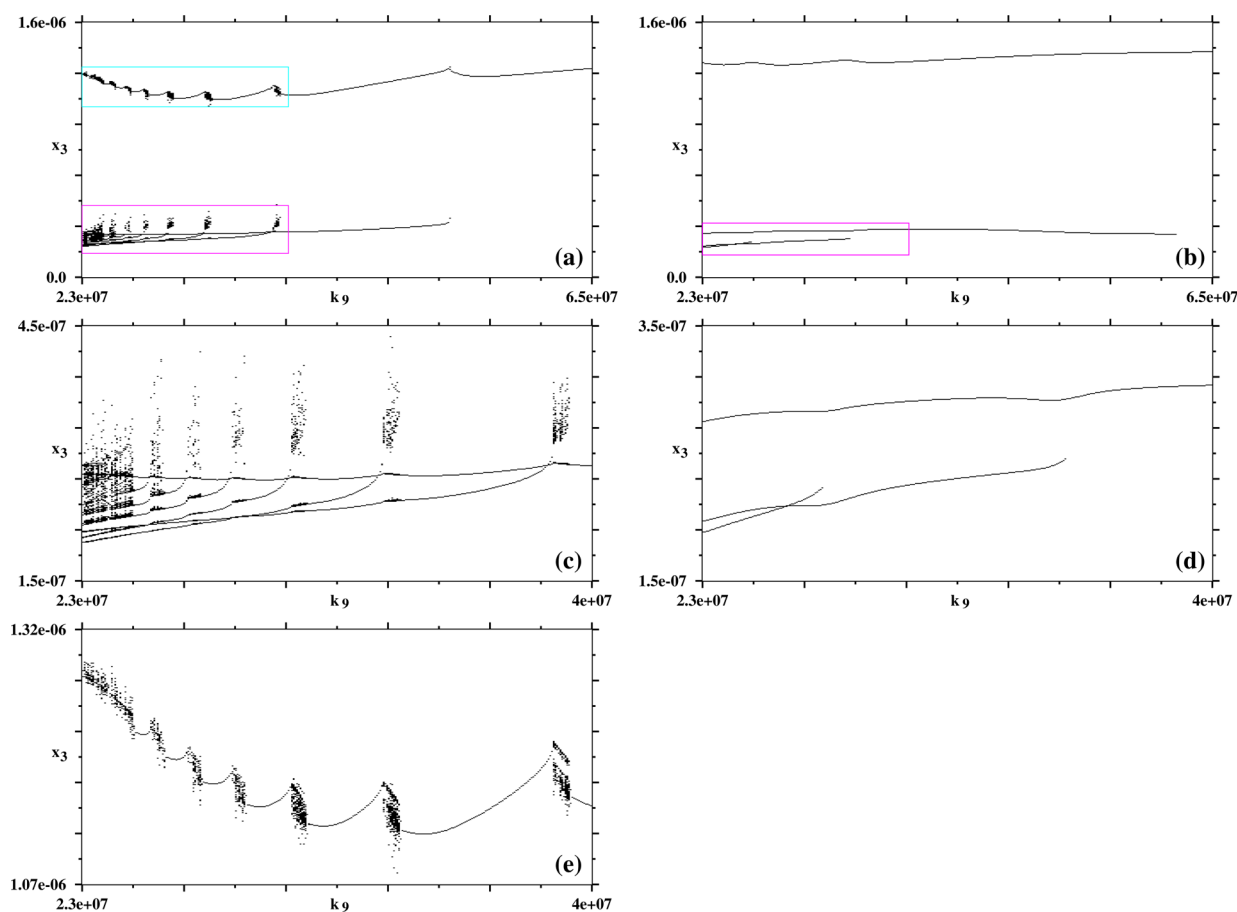


Figure 2. Comparison of bifurcation diagrams for the classical chaos-mediated MMOs along line B of Figure 1 (left column) and the new nonchaos-mediated MMOs along line C (right column). Panels (c) and (d) show magnifications at low Per^{6+} concentrations, and (e) shows that at high Per^{6+} concentration. The bifurcation diagrams were obtained by calculating the maxima of the concentrations of Per^{6+} (variable x_3) oscillations at different values of the pH-dependent rate constant of the NAD^+ dimerization, k_9 .

By contrast, at lower values of k_{12} , that is, at lower supply rates of NADH, a quite distinct organization of MMO states is found, for instance, along the two-parameter path C, defined by $k_{12} = -8.80952 \times 10^{-16} \text{ M}^2 \times k_9 + 1.2226 \times 10^{-7} \text{ M s}^{-1}$. Along this path, the peak-adding scenario between the L^S and L^{S+1} MMO domains is *not* mediated by any chaotic window. Instead, these MMO domains are delimited by a common boundary across which transitions occur via continuous deformations that create and destroy peaks in periodic oscillations in a similar way as recently described for the infinite-dimensional Mackey–Glass delayed feedback system³⁷ and for a CO_2 laser with feedback.³⁸ As k_9 is decreased, the bifurcation diagram plotted along line C in Figure 1 spans from a domain of 1^0 oscillations to a domain of 1^3 oscillations, always showing smooth transitions between adjacent domains. At each transition, the number of small-amplitude peaks changes, whereas the amplitude of the large-amplitude peak remains essentially unaffected during the transition (Figure 2).

Figure 2 presents bifurcation diagrams along the two-parameter paths B and C, corroborating the two scenarios already described for Figure 1, namely, the chaos-mediated and the nonchaos-mediated MMOs. Figure 2a,c,e depicts bifurcations along line B in Figure 1, showing that each transition $1^S \rightarrow 1^{S+1}$ is mediated by a domain of chaotic oscillations. Note that there is a jump in amplitude of the large-amplitude oscillation as the system enters the chaotic window located between adjacent MMO states. Such jumps are typical for the

classical organization of MMOs and correspond to known scenarios obtained numerically^{24,35} and experimentally in the PO reaction.^{21–24} Analogously, Figure 2b,d shows bifurcation diagrams calculated along the two-parameter path C that corroborate the new, nonchaos-mediated MMO scenario, namely, that transitions between 1^S and 1^{S+1} domains occur in the absence of windows of chaos. Interestingly, the magnitude of the large-amplitude oscillations is barely affected when the system changes from a 1^S to a 1^{S+1} MMO following the nonchaos-mediated route.

The transition from the chaos-mediated to the nonchaos-mediated MMO scenarios takes place at a certain boundary located between the lines B and C in Figure 1. When approaching this borderline from B to C, that is, from the side of the classical MMOs, the pattern of the oscillations inside of the chaotic window found in between two adjacent MMO states 1^S and 1^{S+1} changes. The closer the border is approached, the tinier the variations become between the large- and small-amplitude oscillations in the chaotic MMOs. This observation is in good agreement with the finding of Bronnikova et al.,³⁵ who reported that the transitional chaotic dynamics is generated via tori that undergo homoclinic bifurcations to chaos and that these tori become progressively “fatter” as k_9 is decreased. This “fat torus scenario” shows that as k_9 is decreased, the variation in amplitude of chaotic oscillations also decreases, as corroborated by our bifurcation diagrams.

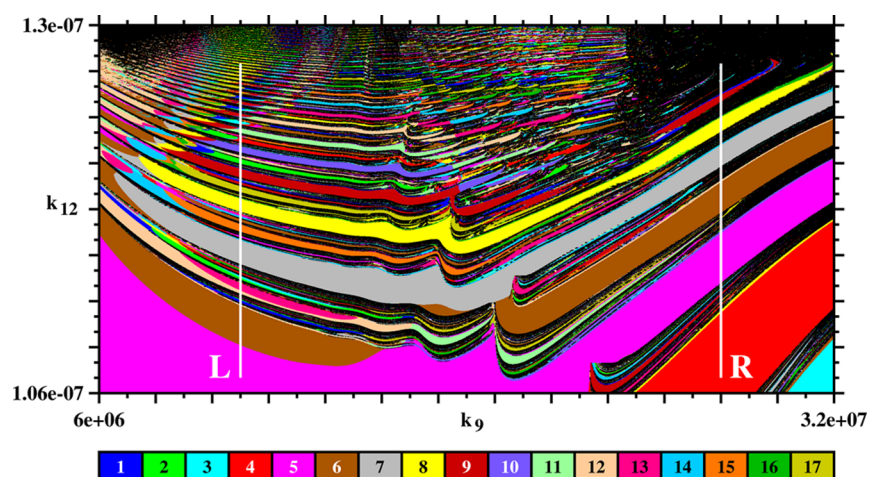


Figure 3. Magnification of the white box in Figure 1 showing a complex mosaic of stable phases of oscillations of distinct multiplicity. Along lines L ($k_9 = 1.1 \times 10^7 \text{ M}^{-1} \text{ s}^{-1}$) and R ($k_9 = 2.8 \times 10^7 \text{ M}^{-1} \text{ s}^{-1}$), one finds chaos-mediated MMO sequences. Bifurcation diagrams calculated along these lines are presented in Figure 4. Note that there is a fault running halfway between lines L and R. The bifurcation diagram shown here is spanned by the rate constant of the pH-sensitive NAD^+ dimerization, k_9 , and the NADH influx rate, k_{12} .

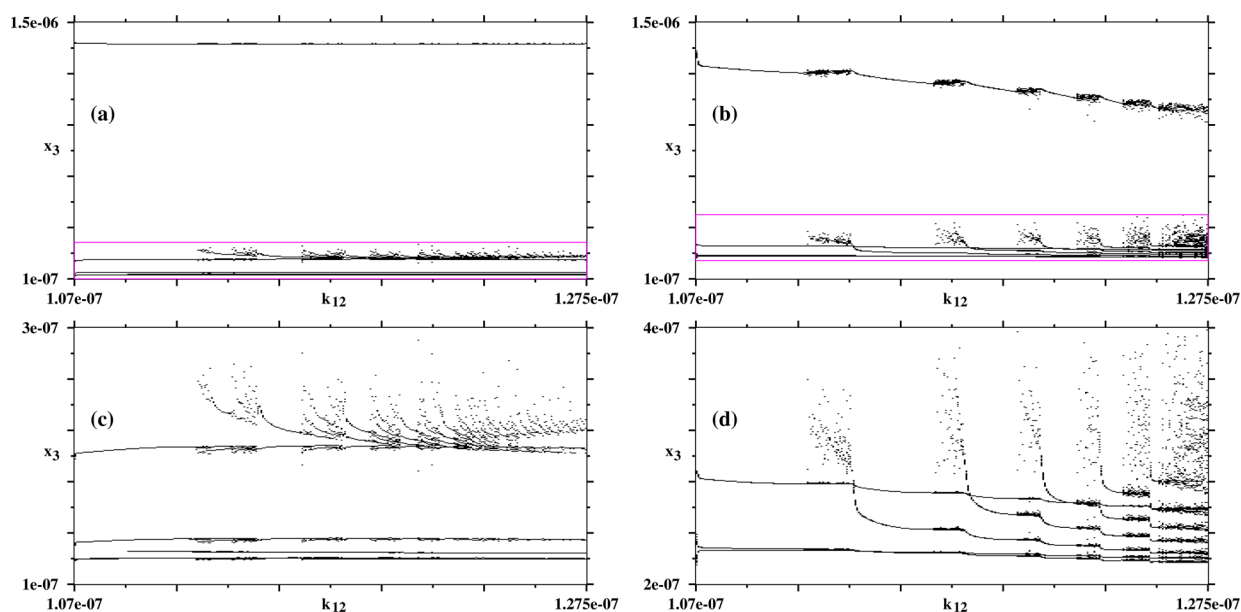


Figure 4. Bifurcation diagrams along the lines (a) L and (b) R of Figure 3. Magnifications of the domains of low x_3 (i.e., Per^{6+}) concentrations along (c) line L and (d) line R. Bifurcations along lines L and R show both the classical chaos-mediated MMOs. The bifurcation diagrams were obtained by calculating the maxima of the concentrations of Per^{6+} (variable x_3) oscillations at different values of the NADH supply rate, k_{12} .

Figure 3 shows a magnification of the region inside of the white box drawn in Figure 1. This region contains a rather complex alternation of MMO sequences mediated by (black) stripes of chaos. Each of the MMO states unfolds via successive peak-doublings as k_{12} is increased, eventually giving way to a narrow window of chaos. As the bifurcation parameter is varied further, the chaotic window gives way to a new MMO state. This motif is repeated in each MMO window along increasing values of k_{12} . For reference, Figure 3 contains two vertical lines, L and R. Bifurcation diagrams along the close neighborhood of such lines look relatively similar, showing typical features of the classical MMOs, although small differences can be noticed in specific places. Interestingly, Figure 3 shows a fault running roughly halfway between lines L and R.

Figure 4a,b shows bifurcation diagrams computed along the vertical lines L and R, respectively. They corroborate the

unfolding described for Figure 3, showing the presence of peak-adding sequences, where subsequent MMOs 1^S and 1^{S+1} are separated by chaotic windows (Figure 4c,d).

The main difference in the bifurcation diagrams along lines L and R (Figure 4a and b, respectively) is found in the behavior of the large-amplitude peaks. While in the bifurcation diagram along line R the magnitude of the large-amplitude oscillation decreases as the number of small-amplitude oscillations S per MMO increases (Figure 4b), the magnitude of the high-amplitude oscillations remains unaffected when the bifurcation diagram is calculated along line L (Figure 4a).

We performed a detailed classification of the oscillatory behaviors, periodic or not, supported by the BFSO model of the PO enzyme reaction. The model aims at a detailed description of the enzyme reaction system, and it has a fairly high dimension when compared to models so far considered in

other disciplines, in studies involving phase diagrams in parameter space. Here, we focused on the k_9, k_{12} control parameter plane because this is the control plane that has been extensively studied^{24,35} and compared with experiments run at different pH values.^{23,24} Our phase diagrams show precisely where the number of spikes changes as a function of the control parameters. From Figure 1, one sees that the parameter region containing the classical chaos-mediated MMOs is essentially confined to the upper right portion of the figure, above the diagonal parallel to line C, namely, the region of larger values of k_9 and k_{12} . Below said diagonal, one predominantly finds nonchaos-mediated MMOs. The parameter space partition into chaos-mediated and nonchaos-mediated MMOs domains is robust. We also report that the control parameter space contains an interesting region where several MMO sequences accumulate, as shown in Figure 3. In fact, in this region, the complexity increases as MMO sequences unfold in a rather complicated way. This complexity defies a systematic description other than by graphical means.

The numerical calculations required very long transients due to the selected initial conditions, which were chosen such as to mimic the beginning of an experiment. On the other hand, the relatively long transient and integration times detailed in the Computational Details were dictated by the rich dynamical sequence of MMOs in the parameter window of Figure 3 and were selected so as to generate diagrams robust against changes of the integrator step size. Outside such window, MMOs stabilize considerably quicker, with transient and integration times reduced by a factor of 5 producing diagrams showing no dependence on the integrator step size. We remark that, currently, there is no method to locate stability phases analytically for arbitrary oscillations, so that the only way to find them is by direct numerical computations.

There are a number of enticing open problems associated with the stability diagrams reported here. From the point of view of applications, they provide reference charts against which one may compare phase diagrams computed for other models and, quite importantly, compare experimentally obtained diagrams. Thus, our stability diagrams can contribute to find possible limitations of both the underlying theoretical framework and its associated reaction mechanisms. Whereas the classical chaos-mediated MMO sequences have already been confirmed experimentally in the PO reaction,^{21–24} the new nonchaos-mediated unfolding reported here remains to be observed in experiments. We believe the experimental confirmation of the nonchaos-mediated MMO unfolding at lower values of k_{12} to present an interesting and rewarding challenge.

As already pointed out, the BFSO model contains a large number of variables. To assess the structural stability of both the model for the PO reaction and that of the nonchaos-mediated MMO sequences, we have started to study simplified versions of the reaction mechanism, for which reduced versions with 8, 7, and 6 independent variables are available.³⁴ We hope also to elucidate which modifications in the dynamics are brought about by the simplification of the model, thus allowing one to access the “price” to be paid for working with reduced models of the PO reaction. These results will be reported elsewhere.

■ COMPUTATIONAL DETAILS

The BFSO model (Table 1) translates into the following differential equations

$$\dot{x}_1 = k_2 x_4 x_{10} - k_3 x_1 x_6 + k_8 x_3 x_5 \quad (1)$$

$$\dot{x}_2 = k_3 x_1 x_6 - k_4 x_2 x_6 \quad (2)$$

$$\dot{x}_3 = -k_8 x_3 x_5 + k_{11} x_7 x_9 + k_6 x_8 x_{10} \quad (3)$$

$$\dot{x}_4 = k_1 x_6 x_7 + k_7 x_8^2 - k_2 x_4 x_{10} \quad (4)$$

$$\dot{x}_5 = k_3 x_1 x_6 + k_4 x_2 x_6 - k_5 x_5 x_7 - k_8 x_3 x_5 - 2k_9 x_5^2 - k_{10} x_5 x_{10} \quad (5)$$

$$\dot{x}_6 = -k_1 x_6 x_7 - k_3 x_1 x_6 - k_4 x_2 x_6 + k_{12} \quad (6)$$

$$\dot{x}_7 = -k_1 x_6 x_7 - k_5 x_5 x_7 + k_7 x_8^2 - k_{11} x_7 x_9 - k_{-13} x_7 + k_{13} [\text{O}_2]_{\text{eq}} \quad (7)$$

$$\dot{x}_8 = k_5 x_5 x_7 - 2k_7 x_8^2 - k_6 x_8 x_{10} \quad (8)$$

$$\dot{x}_9 = k_{10} x_5 x_{10} - k_{11} x_7 x_9 \quad (9)$$

$$\dot{x}_{10} = -k_2 x_4 x_{10} + k_4 x_2 x_6 - k_6 x_8 x_{10} - k_{10} x_5 x_{10} \quad (10)$$

The correspondence between phase-space variables x_i and chemical species is $x_1 \leftrightarrow \text{Per}^{5+}$, $x_2 \leftrightarrow \text{Per}^{4+}$, $x_3 \leftrightarrow \text{Per}^{6+}$, $x_4 \leftrightarrow \text{H}_2\text{O}_2$, $x_5 \leftrightarrow \text{NAD}^*$, $x_6 \leftrightarrow \text{NADH}$, $x_7 \leftrightarrow \text{O}_2$, $x_8 \leftrightarrow \text{O}_2^-$, $x_9 \leftrightarrow \text{Per}^{2+}$, and $x_{10} \leftrightarrow \text{Per}^{3+}$. Here, Per^{n+} denotes the oxidation state of the enzyme peroxidase, and the oxygen solubility limit in solution, $[\text{O}_2]_{\text{eq}}$, is 1.2×10^{-5} M. The initial conditions were chosen such that $(x_1, x_2, \dots, x_9) = 0.0$ and $x_{10} = 1.5 \times 10^{-6}$ M. Under these conditions, the initial value of x_{10} determines the total enzyme concentration present in the reaction system. The initial conditions reproduce the situation at the beginning of an experiment, where the reactor only contains the enzyme (Per^{3+} , variable x_{10}), and the other two reactants (NADH and O_2) begin to be fed to the reactor (mimicked by k_{12} and k_{13} , respectively).

To produce phase diagrams, the parameter window of interest is covered with a mesh of typically 1200×1200 equidistant points. Then, for each point, the temporal evolution is obtained by integrating numerically eqs 1–10 using the standard fourth-order Runge–Kutta algorithm with fixed time step of $h = 0.005$. In Figures 1 and 3, integrations were performed horizontally from right to left starting from the chosen initial conditions $(x_1, x_2, \dots, x_9) = 0.0$ and $x_{10} = 1.5 \times 10^{-6}$ M and proceeding by following the attractor, namely, by using the values of x_i obtained at the rightmost end (when finishing the calculation of a horizontal line) to start the calculation for a new horizontal line, after incrementing the parameter vertically. The first 7×10^5 integration steps were disregarded as a transient time needed to approach the attractor, with the subsequent 140×10^5 steps used to compute up to 800 extrema (maxima and minima) of the variable of interest, x_3 (or Per^{6+}) here, and checking whether peaks repeated or not. The number of spikes in one period of oscillations was then displayed in the so-called isospike diagrams,^{18,39–44} namely, a diagram obtained by counting the number of peaks (local maxima) contained in one period of the periodic oscillations of a variable of interest. All isospike diagrams represent spikes using a palette of 17 colors. Solutions having more than 17 spikes were plotted by recycling the 17 basic colors “modulo 17”, namely, by assigning them a color index given by the remainder of the integer division of the number of peaks by 17. Multiples of 17 are given the index 17. Black is used to represent chaos (i.e., lack of

numerically detectable periodicity), and white and gold mark constant (i.e., nonoscillatory) solutions, if any, having respectively nonzero or zero amplitudes of x_3 , the variable under consideration.

AUTHOR INFORMATION

Corresponding Author

*E-mail: marcus.hauser@ovgu.de or hauser_marcus@web.de.

Notes

The authors declare no competing financial interest.

ACKNOWLEDGMENTS

This work was supported by the Max-Planck Institute for the Physics of Complex Systems, Dresden, in the framework of the Advanced Study Group on Optical Rare Events, and by the Deutsche Forschungsgemeinschaft through the Cluster of Excellence *Engineering of Advanced Materials*. J.A.C.G. was also supported by CNPq, Brazil. All computations were done in the CESUP-UFRGS clusters in Porto Alegre, Brazil.

REFERENCES

- (1) Ostwald, W. Periodische Erscheinungen bei der Auflösung des Chroms in Säuren. *Z. Phys. Chem.* **1900**, *35*, 33–76.
- (2) Field, R. J.; Burger, M., Eds. *Oscillations and Traveling Waves in Chemical Systems*; Wiley: New York, 1985.
- (3) Kapral, R.; Showalter, K., Eds. *Chemical Waves and Patterns*; Kluwer: Dordrecht, The Netherlands, 1995.
- (4) Taylor, A. F. Mechanism and Phenomenology of an Oscillating Chemical Reaction. *Prog. React. Kinet. Mech.* **2002**, *27*, 247–325.
- (5) Iglesias, C.; Meunier, C.; Manuel, M.; Timofeeva, Y.; Delestrée, N.; Zytnicki, D. Mixed Mode Oscillations in Mouse Spinal Motoneurons Arise from a Low Excitability State. *J. Neurosci.* **2011**, *31*, 5829–5840.
- (6) Golomb, D. Mechanism and Function of Mixed-Mode Oscillations in *Vibrissa* Motoneurons. *PLoS One* **2014**, *9*, e109205.
- (7) Erchova, I.; McGonigle, D. J. Rhythms of the Brain: An Examination of Mixed Mode Oscillation Approaches to the Analysis of Neurophysiological Data. *Chaos* **2008**, *18*, 015115.
- (8) Kummer, U.; Olsen, L. F.; Dixon, C. J.; Green, A. K.; Bornberg-Bauer, E.; Baier, G. Switching from Simple to Complex Oscillations in Calcium Signaling. *Biophys. J.* **2000**, *79*, 1188–1195.
- (9) Rotstein, G.; Kuske, R. Localized and Asynchronous Patterns via Canards in Coupled Calcium Oscillators. *Phys. D* **2006**, *215*, 46–61.
- (10) Schmitz, R. A.; Graziani, K. R.; Hudson, J. L. Experimental Evidence of Chaotic States in the Belousov–Zhabotinskii Reaction. *J. Chem. Phys.* **1977**, *67*, 3040–3044.
- (11) Showalter, K.; Noyes, R. M.; Bar-Eli, K. A Modified Oregonator Model Exhibiting Complex Limit Cycle Behavior in a Flow System. *J. Chem. Phys.* **1978**, *69*, 2514–2524.
- (12) Maselko, J.; Swinney, H. L. Complex Periodic Oscillations and Farey Arithmetic in the Belousov–Zhabotinskii Reaction. *J. Chem. Phys.* **1986**, *85*, 6430–6441.
- (13) Kim, K.-R.; Shin, K. J.; Lee, D. J. Complex Oscillations in a Simple Model of the Briggs–Rauscher Reaction. *J. Chem. Phys.* **2004**, *121*, 2664–2672.
- (14) Bakeš, D.; Schreiberová, L.; Schreiber, I.; Hauser, M. J. B. Mixed-Mode Oscillations in a Homogeneous pH-Oscillatory Chemical Reaction System. *Chaos* **2008**, *18*, 015102.
- (15) Hauser, M. J. B.; Fricke, N.; Storb, U.; Müller, S. C. Periodic and Bursting pH Oscillations in an Enzyme Model Reaction. *Z. Phys. Chem.* **2002**, *216*, 375–390.
- (16) Kovacs, C.; Leda, M.; Vanag, V. K.; Epstein, I. R. Small-Amplitude and Mixed-Mode pH Oscillations in the Bromate–Sulfite–Ferrocyanite–Aluminium(III) System. *J. Phys. Chem. A* **2009**, *113*, 146–156.
- (17) Baba, N.; Krischer, K. Mixed-Mode Oscillations and Cluster Patterns in an Electrochemical Relaxation Oscillator under Galvanostatic Control. *Chaos* **2008**, *18*, 015103.
- (18) Nascimento, M. A.; Gallas, J. A. C.; Varela, H. Self-Organized Distribution of Periodicity and Chaos in an Electrochemical Oscillator. *Phys. Chem. Chem. Phys.* **2011**, *13*, 441–446.
- (19) Bi, W.; Hu, Y.; Cabral, M. F.; Varela, H.; Yang, J.; Jiang, R.; Gao, Q. Oscillatory Electro-oxidation of Thiosulfate on Gold. *Electrochim. Acta* **2014**, *133*, 308–315.
- (20) Steinmetz, C. G.; Larter, R. The Quasiperiodic Route to Chaos in a Model of the Peroxidase–Oxidase Reaction. *J. Chem. Phys.* **1991**, *94*, 1388–1396.
- (21) Hauck, T.; Schneider, F. W. Mixed Mode and Quasiperiodic Oscillations in the Peroxidase–Oxidase Reaction. *J. Phys. Chem.* **1993**, *97*, 391–397.
- (22) Hauck, T.; Schneider, F. W. Chaos in a Farey Sequence through Period Doubling in the Peroxidase–Oxidase Reaction. *J. Phys. Chem.* **1994**, *98*, 2072–2077.
- (23) Hauser, M. J. B.; Olsen, L. F. Mixed-Mode Oscillations and Homoclinic Chaos in an Enzyme Reaction. *J. Chem. Soc., Faraday Trans.* **1996**, *92*, 2857–2863.
- (24) Hauser, M. J. B.; Olsen, L. F.; Bronnikova, T. V.; Schaffer, W. M. Routes to Chaos in the Peroxidase–Oxidase Reaction: Period-Doubling and Period-Adding. *J. Phys. Chem. B* **1997**, *101*, 5075–5083.
- (25) Desroches, M.; Guckenheimer, J.; Krauskopf, B.; Kuehn, C.; Osinga, H. M.; Wechselberg, M. Mixed-Mode Oscillations with Multiple Time Scales. *SIAM Rev.* **2012**, *54*, 211–288.
- (26) Bröns, M.; Kaper, T. J.; Rotstein, H. G. Introduction to Focus Issue: Mixed Mode Oscillations: Experiment, Computation, And Analysis. *Chaos* **2008**, *18*, 015101.
- (27) Rinzel, J.; Ermentrout, G. B. In *Methods in Neuromodelling: From Synapses to Networks*; Koch, C., Segev, I., Eds.; MIT Press: Cambridge, MA, 1989; pp 251–292.
- (28) Izhikevich, E. M. Neural Excitability, Spiking and Bursting. *Int. J. Bifurcation Chaos* **2000**, *10*, 1171–1267.
- (29) Scheeline, A.; Olson, D. L.; Williksen, E. P.; Horras, G. A.; Klein, M. L.; Larter, R. The Peroxidase–Oxidase Oscillator and Its Constituent Chemistries. *Chem. Rev.* **1997**, *97*, 739–756.
- (30) Hung, Y.-F.; Schreiber, I.; Ross, J. New Reaction Mechanism for the Oscillatory Peroxidase–Oxidase Reaction and Comparison with Experiments. *J. Phys. Chem.* **1995**, *99*, 1980–1987.
- (31) Bronnikova, T. V.; Fed'kina, V. R.; Schaffer, W. M.; Olsen, L. F. Period-Doubling Bifurcations and Chaos in a Detailed Model of the Peroxidase–Oxidase Reaction. *J. Phys. Chem.* **1995**, *99*, 9309–9312.
- (32) Larter, R.; Hemkin, S. Further Refinements of the Peroxidase–Oxidase Oscillator Mechanism: Mixed-Mode Oscillations and Chaos. *J. Phys. Chem.* **1996**, *100*, 18924–18930.
- (33) Schaffer, W. M.; Bronnikova, T. V.; Olsen, L. F. Nonlinear Dynamics of the Peroxidase–Oxidase Reaction. II. Compatibility of an Extended Model with Previously Reported Model-Data Correspondences. *J. Phys. Chem. B* **2001**, *105*, 5331–5340.
- (34) Straube, R.; Flockerzi, D.; Müller, S. C.; Hauser, M. J. B. Reduction of Chemical Reaction Networks by Quasi-Integrals. *J. Phys. Chem. A* **2005**, *109*, 441–450.
- (35) Bronnikova, T. V.; Schaffer, W. M.; Hauser, M. J. B.; Olsen, L. F. Routes to Chaos in the Peroxidase–Oxidase Reaction. II: The Fat Torus Scenario. *J. Phys. Chem. B* **1998**, *102*, 632–640.
- (36) Bronnikova, T. V.; Schaffer, W. M.; Olsen, L. F. Quasiperiodicity in a Detailed Model of the Peroxidase–Oxidase Reaction. *J. Chem. Phys.* **1996**, *105*, 10849–10859.
- (37) Junges, L.; Gallas, J. A. C. Intricate Routes to Chaos in the Mackey–Glass Delayed Feedback System. *Phys. Lett. A* **2012**, *376*, 2109–2116.
- (38) Junges, L.; Gallas, J. A. C. Frequency and Peak Discontinuities Observed in Self-Pulsations of a CO₂ Laser with Feedback. *Opt. Commun.* **2012**, *285*, 4500–4506.
- (39) Freire, J. G.; Gallas, J. A. C. Stern–Brocot Trees in the Periodicity of Mixed-Mode Oscillations. *Phys. Chem. Chem. Phys.* **2011**, *13*, 12191–12198.

(40) Freire, J. G.; Gallas, J. A. C. Stern–Brocot Trees in Cascades of Mixed-Mode Oscillations and Canards in the Extended Bonhoeffer–van der Pol and the FitzHugh–Nagumo Models of Excitable Systems. *Phys. Lett. A* **2011**, *375*, 1097–1103.

(41) Freire, J. G.; Pöschel, T.; Gallas, J. A. C. Stern–Brocot Trees in Spiking and Bursting of Sigmoidal Maps. *Europhys. Lett.* **2012**, *100*, 48002.

(42) Souza, S. L. T.; Lima, A. A.; Caldas, I. R.; Medrano-T, R. O.; Guimarães-Filho, Z. O. Self-Similarities of Periodic Structures for a Discrete Model of a Two-Gene System. *Phys. Lett. A* **2012**, *376*, 1290–1294.

(43) Gallas, M. R.; Gallas, M. R.; Gallas, J. A. C. Distribution of Chaos and Periodic Spikes in a Three-Cell Population Model of Cancer. *Eur. Phys. J.: Spec. Top.* **2014**, *223*, 2131–2144.

(44) Hoff, A.; da Silva, D. T.; Manchein, C.; Albuquerque, H. A. Bifurcation Structures and Transient Chaos in a Four-Dimensional Chua Model. *Phys. Lett. A* **2014**, *378*, 171–177.